Radiation in spherically symmetric structures. II. Enhancement and inhibition of dipole radiation in a spherical Bragg cavity

Kevin G. Sullivan and Dennis G. Hall
The Institute of Optics, University of Rochester, Rochester, New York 14627
(Received 7 February 1994)

Utilizing a classical model, the interaction of a centrally positioned radiating dipole with a finite-sized spherical Bragg structure is treated. A straightforward approach is adopted to calculate the radiative lifetime and resonance frequency shifts of a source within a three-dimensional Bragg structure, and applied to a simple physical system that can be expected to provide a good estimate of the finite-size effects that will occur in more complicated structures. These calculations are of fundamental theoretical interest for understanding dipole-surface interactions, particularly in spherical geometries requiring a vector formulation. The work is of potential practical interest as applied to spherical cavity and photonic structure design, and stresses the connection between recent photonic band-gap research and the earlier investigations of dipole-mirror interactions.

PACS number(s): 42.60.Da, 03.50.De, 41.20.Jb

I. INTRODUCTION

It is well understood that the presence of an interface or structure can significantly impact the characteristic behavior of a radiating system [1,2]. Specifically, the radiative decay rate and resonance frequency of a radiating system depend on the electromagnetic modes (or states) associated with the surrounding environment. This dependence is expected as radiative properties are not inherent to an isolated atom but characteristic of an atom coupled to a physical system. For an isolated atom in a vacuum, an infinity of states exist which are available to the radiated photon. By modifying these states through the presence of an interface or cavity, the radiative properties of excited atoms can be strongly modified. Systems that change the density of modes are currently of great interest in the fields of photonics and quantum electrodynamics.

The origins of this renewed interest can be traced to earlier investigations concerned with the effects of metal and dielectric interfaces, and metallic waveguides near cutoff, on atomic radiation [3,4]. A series of experiments by Drexhage [5] and others demonstrated the strong dependence of the fluorescent lifetime of molecules on the separation between the molecule and a conducting surface. The experimental shift in the resonance frequency of an electric dipole near a conducting surface was demonstrated by Holland and Hall [6]. Due to the inherent lossy nature of metallic structures, recent investigations have considered periodic dielectric structures. The structures considered incorporate one-dimensional and three-dimensional rectangular periodicities. The one-dimensional case is applicable to vertical-cavity surface-emitting semiconductor lasers [7–9]. The three-dimensional (3D) case offers the possibility of a total photonic band gap, i.e., an energy band of nonzero width in which electromagnetic wave propagation is isotropically forbidden [10]. Two-dimensional periodic structures have also received considerable interest [11,12].

For multidimensional systems, previous research focused on energy gap calculations for translationally invariant systems. The objective is to use a periodic refractive index (Bragg structure) to produce a photonic band structure, which is analogous to the periodic potential energy in a crystalline solid which produces an electronic band structure. A source placed within such a periodic medium would find no channels for radiative decay for frequencies that fall within the forbidden frequency gaps. Radiation at those frequencies would thus be inhibited.

Most photonic band-structure calculations considered systems that are infinite in extent, a condition needed for complete inhibition of the source radiation, but one not easily realized in experiments. A 3D Bragg reflecting structure at optical frequencies has a fundamental length scale set by the optical wavelength in the material, typically a few thousand angstroms. A structure at least several times that length along each spatial direction will be required to achieve a strong Bragg reflection and hence strong enhancement or inhibition effects. Experiments designed to measure the radiative lifetime face fabrication issues that limit the size of available samples and hence the size of the effects that can be obtained. Future applications in optoelectronics can also be expected to place upper limits on the sizes of acceptable structures. It is therefore important to understand quantitatively the degree to which finite-size structures can inhibit or enhance the radiative decay rate.

In this paper, we investigate the radiative properties of a dipole placed at the center of a concentric spherical Bragg structure of finite size. This work extends to three dimensions our earlier investigation of a two-dimensional system: a line source in a cylindrically periodic structure [13]. The spherical Bragg structure is not translationally invariant, so terms such as photonic band structure and band gap are not appropriate. Physically, however, a source placed at the center of this system will experience along all directions the strong Bragg-reflected fields expected to occur in a material that exhibits a true band

 ©1994 The American Physical Society

gap. The reflected fields at the central position in the concentric-spherical system will be at least as large as those at a typical point in a photonic band-gap structure of comparable size. Therefore, it is unlikely that the degree of enhancement or inhibition of the dipole's radiative decay rate in a photonic band-gap material will exceed that in a spherical Bragg cavity of similar size. We provide in this paper a straightforward approach to calculating the radiative lifetime of a source within a 3D Bragg structure and apply it to a simple physical system that can be expected to provide a good estimate of the finite-size effects that will occur in more complicated structures.

The organization of the paper is as follows. In Sec. II, we develop the theoretical formulation to calculate the enhancement and inhibition of radiation from a dipole source in terms of the radiative damping rate (inverse lifetime) and the associated frequency shifts. The formulation utilizes vector spherical coupled-wave theory as detailed in our companion paper to calculate the reflection of the radiated field back onto the source. Using the results of Sec. II, the case of a centrally positioned dipole source in a spherical Bragg cavity is considered in Sec. III. In Sec. IV, the enhancement and inhibition of radiation and frequency shifts are numerically examined for several structures. Finally, in Sec. V, conclusions are drawn from the results of this investigation.

II. THEORY OF RADIATIVE EFFECTS IN A SPHERICAL BRAGG STRUCTURE

A. Source equation of motion

In this subsection, closed-form expressions for the normalized radiative damping rate and the resonance frequency shift are derived via a classical approach. As suggested above, there is a strong connection between the recent work on photonic band-gap structures and the earlier body of work on the problem of radiation from a source placed in front of a metal mirror. The behavior of the radiative lifetime in both cases is well explained, qualitatively and quantitatively, as that of a molecule radiating in the presence of its own reflected field [14]. Adopting this model, we treat the source as a classical dipole that interacts with its own reflected field within the spherical cavity. A source placed within this Bragg-reflecting structure, which plays the role of a three-dimensional mirror with a frequency-dependent reflectivity, is therefore subjected to strong reflected waves that modify the radiative lifetime and resonance frequency of the source.

The above approach was used successfully by Chance, Prock, and Silbey [15] to quantitatively model the radiative lifetime experimental data of Drexhage. The theory as applied to the calculation of resonance frequency shifts was later confirmed experimentally by Holland and Hall [6]. Furthermore, it was shown that this classical frequency shift exactly agrees with the quantum-mechanically calculated level shift for the first excited state when the source is a simple harmonic oscillator [16]. A more realistic atomic model requires a quantum-mechanical calculation to accurately predict the level shift.

The idealized dipole source is modeled as a harmonically bound charge with dipole moment p that obeys the equation of motion

$$\ddot{p}+\omega_0^2 p=\left[\frac{q^2}{m}\right]E_R-b_0\dot{p}\ , \tag{1}$$

where ω_0 is the resonant angular frequency in the absence of all damping, q is the effective charge, m is the effective mass, E_R is the component of the reflected field parallel to the dipole moment orientation at the source position, and b_0 is the damping constant in the core material for $E_R=0$. Equation (1) describes a driven, damped harmonic oscillator, where the external driving force is proportional to the component of the reflected field that does work on the bound charge. The dipole moment p and reflected field component E_R oscillate at the same complex frequency $\Omega=\omega-ib/2$:

$$p=p_0\exp[-i\Omega t]=p_0\exp[-(i\omega+b/2)t]\ , \tag{2a}$$

$$E_R=E_0\exp[-i\Omega t]\ , \tag{2b}$$

where ω and b are the resonance frequency and damping rate in the presence of the cavity, respectively.

Substituting Eqs. (2a) and (2b) into Eq. (1) and equating real and imaginary portions, the following equations result:

$$\frac{b}{b_0}=1+\frac{q^2}{m\omega p_0 b_0}\,\mathrm{Im}(E_0)\ , \tag{3}$$

$$\omega^2-\omega_0^2=\frac{b^2}{4}-\frac{bb_0}{2}-\frac{q^2}{mp_0}\,\mathrm{Re}(E_0)\ . \tag{4}$$

Equation (3) is the expression for the normalized radiative damping rate (inverse of the normalized lifetime). Equation (4) can be simplified by recognizing the relative magnitude of the frequency shift, i.e., $\Delta\omega\equiv\omega-\omega_0\ll\omega,\omega_0$. Using this assumption, which will be examined in detail in Sec. IV, Eq. (4) yields the approximate result

$$\Delta\omega\approx\frac{b^2}{8\omega_0}-\frac{bb_0}{4\omega_0}-\frac{q^2}{2m\omega_0 p_0}\,\mathrm{Re}(E_0)\ . \tag{5}$$

Thus the normalized radiative damping rate and frequency shift are related to the out-of-phase and in-phase components, respectively, of the reflected field which does work on the point dipole source. It is this reflected field that is calculated in the subsequent sections through the application of a coupled-amplitude formalism and electromagnetic boundary conditions. In general, Eqs. (3) and (5) are coupled equations. Approximate, decoupled forms which are valid for a wide range of structures and sources are derived in Sec. II F.

B. Source field

Consider the geometry depicted in Fig. 1 of the preceding paper. We consider an idealized system consisting of a single (point) electric dipole radiator placed at the center of a spherically symmetric Bragg reflector as de-

picted in that figure. The square of the refractive index of the spherical system is constant in the range $0<r<r_1$, varies sinusoidally with period Λ in the range $r_1<r<r_1+L$, and is everywhere continuous. Thus the square of the refractive index can be defined such that

$$n^2(r)=n_0^2+\Delta n^2(r) , \tag{6a}$$

$$\Delta n^2(r)=\begin{cases} Q\sin[2\pi(r-r_1)/\Lambda] & r_1<r<r_1+L \\ 0 \quad \text{otherwise} , \end{cases} \tag{6b}$$

where Q is the amplitude of the modulation in the square of the refractive index and r_1 denotes the beginning of the modulated (Bragg) region. The period Λ is chosen to satisfy the (first-order) Bragg condition at the wavelength λ emitted by the source, i.e., $\Lambda=\lambda/2$ (for $\Delta\omega \ll \omega,\omega_0$).

Having established the system geometry, the objective of this subsection is to determine analytically the source field generated by a point dipole placed at $r=r_0$. The derivation of the source field (subscript S) in the core $(0<r<r_1)$ begins with an examination of the vector wave equation in a homogeneous, unbounded medium. The electric displacement field $\vec{D}_S(\vec{r})$, in the presence of an oscillating current density, is governed by the standard vector wave equation [assuming $\exp(-i\omega_0 t)$ harmonic time dependence]

$$\vec{\nabla}\times\vec{\nabla}\times\vec{D}_S(\vec{r})-\omega_0^2\mu_0\varepsilon\vec{D}_S(\vec{r})=i\mu_0\omega_0\varepsilon\vec{J}(\vec{r}) , \tag{7}$$

where ω_0 is the free-space angular frequency, μ_0 is the assumed constant permeability, and $\varepsilon=\varepsilon_0 n_0^2$ is a constant permittivity. For a point dipole, the current density can be defined such that

$$\vec{J}(\vec{r})=\hat{\vec{\alpha}}\frac{\delta(r-r_0)\delta(\theta-\theta_0)\delta(\varphi-\varphi_0)}{r^2\sin\theta}J_0=\hat{\vec{\alpha}}\delta(\vec{r}-\vec{r}_0)J_0 , \tag{8}$$

where $\hat{\vec{\alpha}}$ is a unit vector denoting the dipole moment orientation, $\delta(\vec{r}-\vec{r}_0)$ is the three-dimensional Dirac delta function, and J_0 is a parameter denoting source strength.

The general integral solution to Eq. (7) may be formed such that

$$\vec{D}_S(\vec{r})=i\omega_0\mu_0\varepsilon\int\int\int_V \overleftrightarrow{G}\cdot\vec{J}(\vec{r}')d^3\vec{r}' , \tag{9}$$

where $\overleftrightarrow{G}(\vec{r},\vec{r}')$ is the dyadic Green's function, which satisfies

$$\vec{\nabla}\times\vec{\nabla}\times\overleftrightarrow{G}(\vec{r},\vec{r}')-k^2\overleftrightarrow{G}(\vec{r},\vec{r}')=\overleftrightarrow{I}\delta(\vec{r}-\vec{r}') , \tag{10}$$

where $k=(\mu_0\varepsilon)^{1/2}\omega_0$, and the appropriate boundary conditions discussed below. In the above equation, $\overleftrightarrow{I}$ is the unit dyad defined such that $\overleftrightarrow{I}\cdot\vec{V}=\vec{V}\cdot\overleftrightarrow{I}=\vec{V}$ for any vector field $\vec{V}$. The solution to Eq. (10) can be found subject to the Sommerfeld radiation condition, i.e., purely outgoing waves as the radial variable r approaches infinity. For this physical boundary condition, the analytical form for the dyadic Green's function is given by [17]

$$\overleftrightarrow{G}(\vec{r},\vec{r}')=[\overleftrightarrow{I}+\vec{\nabla}\vec{\nabla}]g(\vec{r},\vec{r}') , \tag{11}$$

where $g(\vec{r},\vec{r}')$ is the three-dimensional scalar Green's function with the familiar form

$$g(\vec{r},\vec{r}')=\frac{e^{ik|\vec{r}-\vec{r}'|}}{4\pi|\vec{r}-\vec{r}'|} . \tag{12}$$

While the above development is strictly valid for an unbounded, homogeneous region, a reciprocity argument can be used to prove equivalence for a bounded, homogeneous region [17]. Thus, substituting explicit forms for the dyadic Green's function and current density, Eq. (9) reduces to give the electric displacement field in the source region

$$\vec{D}_S(\vec{r})=i\omega_0\mu_0\varepsilon J_0\left[g(\vec{r},\vec{r}_0)\hat{\vec{\alpha}}+\frac{1}{k^2}\vec{\nabla}\{\vec{\nabla}g(\vec{r},\vec{r}_0)\cdot\hat{\vec{\alpha}}\}\right] . \tag{13}$$

Furthermore, the magnetic field is determined by an application of Maxwell's equations which yields the result

$$\vec{B}_S(\vec{r})=\vec{\nabla}\times\{\mu_0 J_0 g(\vec{r},\vec{r}_0)\hat{\vec{\alpha}}\} . \tag{14}$$

Note that the source fields have a singularity at the source point $\vec{r}=\vec{r}_0$, which is typical for a point-dipole field expansion. This singularity will not pose a problem as subsequent calculations involve only the reflected field evaluated at the source position. In general, the field components generated by a point dipole can be expressed as a dyadic differential operator of the field variables acting upon the scalar Green's function.

As detailed in our companion paper, the field description in the Bragg region of the structure involves an intuitively appealing coupled-amplitude formalism of inward- and outward-traveling spherical waves. Thus the scalar Green's function is expandable in terms of spherical waves such that

$$g(\vec{r},\vec{r}_0)=ik\sum_{l=0}^{\infty}\sum_{m=-l}^{l} j_l(kr_<)h_l^{(1)}(kr_>)Y_{lm}(\theta,\varphi)\times Y_{lm}^*(\theta_0,\varphi_0)=\frac{ik}{4\pi}h_0^{(1)}(k|\vec{r}-\vec{r}_0|) , \tag{15}$$

where $r_>$ ($r_<$) is the greater (lesser) of r and r', and spherical Bessel, Hankel, and harmonic functions have been used. While Eq. (15) is an infinite series, only a finite number of terms is necessary in practice to evaluate Eqs. (13) and (14) at any field point ($\vec{r}\neq\vec{r}_0$) for a given dipole position. This is due to the numerical convergence of the spherical Bessel and Hankel function product.

C. Construction of the total field in the source region

The field solutions in the core and the Bragg regions have been examined separately in Sec. II B above and in our companion paper, respectively. The remaining task is to combine these independent calculations through the application of electromagnetic boundary conditions to obtain the reflected fields in the core region. Returning to the source field, Eq. (13) can be rewritten in the form

$$\vec{D}_S(\vec{r})=-\omega_0\mu_0\varepsilon k J_0(\overleftrightarrow{I}+\vec{\nabla}\vec{\nabla})g(\vec{r},\vec{r}_0)\cdot\hat{\vec{\alpha}} . \tag{16}$$

As noted above, $D_S(\vec{r})$ can be expressed as a dyadic differential operator acting upon the scalar Green's function. This differential operator acts only upon the field variables (r,θ,φ). Outside the source point, however, Eq. (16) can be recast in a form where the differential operator acts solely upon the source variables. This transformation will later prove fortuitous in the extraction of the transverse field components of the reflected field as detailed in Sec. II E.

Following Ref. [17], we examine the source generated fields in the core region for $\vec{r}\neq\vec{r}_0$. Equation (16) can be alternatively written as

$$\vec{D}_S(\vec{r})=\frac{iJ_0}{\omega_0}\vec{\nabla}\times\vec{\nabla}\times\hat{\vec{\alpha}}g(\vec{r},\vec{r}_0)\ ,\quad \vec{r}\neq\vec{r}_0\ . \tag{17}$$

As demonstrated in our companion paper, only the radial component of the above equation is necessary. For the TM (transverse magnetic with respect to the radial vector) case involving $\vec{D}_S$, the characteristic component outside the source point is given by

$$[\vec{r}\cdot\vec{D}_S(\vec{r})]^{\mathrm{TM}}=\frac{iJ_0}{\omega_0}\vec{r}\cdot\vec{\nabla}\times\vec{\nabla}\times\hat{\vec{\alpha}}g(\vec{r},\vec{r}_0)\ ,\quad \vec{r}\neq\vec{r}_0\ . \tag{18}$$

Using reciprocity arguments and the symmetry property of the scalar Green's function, it can be shown that Eq. (18) is equivalent to the following form:

$$[\vec{r}\cdot\vec{D}_S(\vec{r})]^{\mathrm{TM}}=\frac{iJ_0}{\omega_0}\hat{\vec{\alpha}}\cdot\vec{\nabla}_0\times\vec{\nabla}_0\times\vec{r}_0 g(\vec{r},\vec{r}_0)\ ,\quad \vec{r}\neq\vec{r}_0\ . \tag{19}$$

A similar method can be used for Eq. (14) for the TE (transverse electric with respect to the radial vector) case such that

$$[\vec{r}\cdot\vec{B}_S(\vec{r})]^{\mathrm{TE}}=i\mu_0 J_0\hat{\vec{\alpha}}\cdot\vec{\nabla}_0\times\vec{r}_0 g(\vec{r},\vec{r}_0)\ ,\quad \vec{r}\neq\vec{r}_0\ . \tag{20}$$

Thus the characteristic TE and TM fields generated by the point dipole have been recast in forms where the differential operator acts solely upon the source (zero subscripted) variables. Equations (19) and (20) can be generally written such that

$$[\vec{r}\cdot\vec{V}_S(\vec{r})]=O_S(\vec{r}_0)\sum_{l=0}^{\infty}\sum_{m=-l}^{l} j_l(kr_<)h_l^{(1)}(kr_>)\times Y_{lm}(\theta,\varphi)Y_{lm}^*(\theta_0,\varphi_0)\ ,\quad \vec{r}\neq\vec{r}_0\ , \tag{21}$$

where $O_S(\vec{r}_0)$ is a polarization-dependent differential operator acting on the source variables and the spherical wave expansion [Eq. (15)] for the scalar Green's function has been used.

In the source region, the total radial component of the field can be expressed as the sum of the radial components of the source and reflected fields. This reflected field (subscript R) consists of outward- and inward-going spherical waves generated by reflections from the spherical Bragg structure. The total characteristic field (subscript T) in the core region can be written

$$[\vec{r}\cdot\vec{V}_T(\vec{r})]=[\vec{r}\cdot\vec{V}_S(\vec{r})]+[\vec{r}\cdot\vec{V}_R(\vec{r})]\ , \tag{22}$$

where $[\vec{r}\cdot\vec{V}_S(\vec{r})]$ is given by Eq. (21) and

$$[\vec{r}\cdot\vec{V}_R(\vec{r})]=O_S(\vec{r}_0)\sum_l\sum_m[A_{lm}^{(1)}h_l^{(1)}(kr)+A_{lm}^{(2)}h_l^{(2)}(kr)]Y_{lm}(\theta,\varphi)\ , \tag{23}$$

where $A_{lm}^{(i)}$ are constant outward- and inward-traveling wave amplitudes.

D. Applying the boundary conditions

The constant wave amplitudes can be determined from the boundary conditions on the source region. At the center $r=0$, the sum of all outward-traveling radial waves must be equal to the sum of all inward-traveling radial waves. This boundary condition is necessary to prevent the total field from diverging at the center owing to the singular nature of the spherical Neumann functions. There is still a difficulty if the source is located at the system origin as the generated field is inherently singular at the center of the structure. However, this singularity does not affect the analysis, which is concerned only with the well-behaved reflected field at the source position. This boundary condition is already built into the source field as the lesser of r and r_0 is associated with the nonsingular spherical Bessel function. The application of this central boundary condition for the reflected field [Eq. (23)] requires that

$$A_{lm}^{(1)}=A_{lm}^{(2)}=A_{lm}\ . \tag{24}$$

Equation (24) can be logically interpreted in the context of the closed nature of a spherical geometry where a reflected wave in the central region becomes part of a standing wave. Intuitively, the boundary condition suggests that an inward-going wave becomes an outward-going wave as it passes through the center.

The other boundary condition is applied at the inner radius of the spherical Bragg structure $r=r_1$. It requires that the sum of the inward-traveling radial waves be equal to the sum of the product of the outward-traveling radial waves and the amplitude reflection coefficients ρ_l. Mathematically, this condition assumes the general form to be satisfied at $r=r_1$:

$$\begin{aligned}O_S(\vec{r}_0)\sum_l\sum_m A_{lm}^{(2)}h_l^{(2)}(kr)Y_{lm}(\theta,\varphi)&=O_S(\vec{r}_0)\sum_l\sum_m\rho_l A_{lm}^{(1)}h_l^{(1)}(kr)Y_{lm}(\theta,\varphi)\\&+O_S(\vec{r}_0)\sum_l\sum_m\rho_l j_l(kr_<)h_l^{(1)}(kr_>)\times Y_{lm}(\theta,\varphi)Y_{lm}^*(\theta_0,\varphi_0)\ .\end{aligned} \tag{25}$$

Equation (25) must hold for all r_1 independent of angular position. Thus, multiplying Eq. (25) by $Y_{l'm'}^*(\theta,\varphi)$, integrating over 4π sr, and utilizing the orthogonality relation for the spherical harmonic functions

$$\int_0^{2\pi}\int_0^{\pi}Y_{l'm'}^*(\theta,\varphi)Y_{lm}(\theta,\varphi)\sin\theta' d\theta' d\varphi'=\delta_{ll'}\delta_{mm'}\ , \tag{26}$$

we obtain

$$A_{lm}^{(2)}h_l^{(2)}(kr_1)=\rho_l[\,A_{lm}^{(1)}h_l^{(1)}(kr_1)+j_l(kr_0)h_l^{(1)}(kr_1)Y_{lm}^*(\theta_0,\varphi_0)]\ . \quad (27)$$

In the derivation of Eq. (27), the explicit form of the radial component of the source field [Eq. (21)] was used. The inverse of the linear differential operator $O_S^{-1}(\vec{r}_0)$ was also applied to both sides of Eq. (25). As a consequence of Eq. (26), all the l and m harmonics are decoupled in a spherically symmetric region. The value of the lth-order amplitude reflection coefficient ρ_l is provided by a solution of the coupled-amplitude equations for a particular polarization case in the spherical Bragg region, as discussed in our companion paper. Equations (24) and (27) can be combined to yield the reflected wave amplitude such that

$$A_{lm}=\frac{\rho_l j_l(kr_0)h_l^{(1)}(kr_1)Y_{lm}^*(\theta_0,\varphi_0)}{h_l^{(2)}(kr_1)-\rho_l h_l^{(1)}(kr_1)}\ . \quad (28)$$

Thus, Eq. (23), with the application of Eqs. (24) and (28), fully defines the characteristic radial component of the reflected field.

E. Transverse field components of the reflected field

In most cases, it is necessary to construct the remaining transverse field components to fully define the component of the reflected electric field which does work on the point dipole. The results from our companion paper can be applied to determine these components. The commutation of the angular momentum operator $\vec{L}$ with the source differential operator $O_S(\vec{r}_0)$ is necessary for the validity of the field forms detailed below. This commutation is assured by the reexpression, in Sec. II C, of the source differential operator to the source variable space, which is independent of the field variable space of the angular momentum operator.

Applying the results from the companion paper, and Eqs. (23) and (24), the reflected magnetic field for the TM case is constructed, yielding the expression

$$\vec{B}_R^{\rm TM}=-\mu_0\omega_0 O_S^{\rm TM}(\vec{r}_0)\sum_{l=0}^{\infty}\sum_{m=-l}^{+l}\frac{1}{l(l+1)}2(A_{lm})^{\rm TM}j_l(kr)\times\vec{L}Y_{lm}(\theta,\varphi)\ . \quad (29)$$

The corresponding reflected electric displacement field can be obtained through the application of Maxwell's equations:

$$\vec{D}_R^{\rm TM}=\frac{i}{\mu_0\omega_0}\vec{\nabla}\times\vec{B}_R^{\rm TM}\ . \quad (30)$$

The reflected electric displacement field for the TE case can be similarly determined to yield

$$\vec{D}_R^{\rm TE}=\varepsilon\omega_0 O_S^{\rm TE}(\vec{r}_0)\sum_{l=0}^{\infty}\sum_{m=-l}^{+l}\frac{1}{l(l+1)}2(A_{lm})^{\rm TE}j_l(kr)\times\vec{L}Y_{lm}(\theta,\varphi)\ . \quad (31)$$

Finally, the component of the reflected electric field parallel to the dipole moment orientation at the source position is a linear combination of the TE and TM field solutions such that

$$E_R=(\varepsilon_0 n_0^2)^{-1}\lim_{\vec{r}\to\vec{r}_0}\{\hat{\vec{\alpha}}\cdot[\vec{D}_R^{\rm TE}(\vec{r})+\vec{D}_R^{\rm TM}(\vec{r})]\}\ . \quad (32)$$

It is Eq. (32) that provides the reflected field component required for a calculation of the radiative damping rate and frequency shift of Eqs. (3) and (5), respectively.

F. Radiative damping rate and frequency shift

The preceding subsections provided a formulation for the calculation of the reflected electric-field strength at the source position for a dipole in the core region of a spherical Bragg structure. From Eqs. (3) and (5), it is necessary to calculate b_0, the radiative damping rate in the absence of the structure. This result can be calculated by using a classical radiation reaction argument [18] to yield

$$b_0=n_0\left[\frac{q^2\omega_0^2}{6\pi\varepsilon_0 mc^3}\right]\ , \quad (33)$$

where the additional prefactor of n_0 accounts for the index of the core region. As the normalized radiative damping rate b/b_0 is independent of the absolute source strength, it is also useful to introduce the electric field parameter E_S:

$$E_S=\frac{-\mu_0\omega_0 kJ_0}{6\pi}=\frac{i\mu_0\omega_0^2 p_0 k}{6\pi}\ . \quad (34)$$

J_0 has been replaced by $-i\omega_0 p_0$ in the second expression. Equation (34) collects parameters introduced via Eqs. (13) and (15); a factor of $1/6\pi$ was included to mimic the form of the radiative damping rate in the absence of the Bragg structure.

Substituting Eqs. (33) and (34) into Eq. (3), a simplified expression for the normalized radiative damping rate in the presence of the cavity is obtained:

$$\frac{b}{b_0}=1+{\rm Re}\left[\frac{E_R}{E_S}\right]\ , \quad (35)$$

where the approximation $\omega\approx\omega_0$ was used. Thus the normalized radiative damping rate (inverse normalized lifetime) is proportional to the real part of the reflected electric field normalized by the source strength. Because this normalized reflected field spans the range $(-1,\infty)$, b/b_0 will span the physically meaningful range $(0,\infty)$. As $b/b_0\to 0$, the radiative lifetime becomes large, indicating inhibition of radiation. This limit may be physically interpreted as arising from a vector field node at the source, i.e., the normalized reflected electric field produces an effect equal in magnitude and exactly out-of-phase with the source oscillation, thus canceling the oscillation. As $b/b_0\to\infty$, or when there is a vector field antinode, the radiative lifetime becomes small, indicating enhancement.

The expression for the frequency shift can be reexpressed by substituting Eq. (35) into Eq. (5), yielding

$$\Delta\omega=\frac{b_0^2}{8\omega_0}\left\{\left[\mathrm{Re}\left[\frac{E_R}{E_S}\right]\right]^2-1\right\}+\frac{b_0}{2}\,\mathrm{Im}\left[\frac{E_R}{E_S}\right] . \tag{36}$$

Equation (36) can be simplified by comparing the relative magnitudes of the term coefficients. For example, consider a harmonically oscillating dipole source in free space emitting in the middle of the visible spectrum at $\lambda_0=0.5$ μm. In this case, $\omega_0=0.4\times10^{16}$ Hz and $b_0=8.9\times10^7$ Hz. Therefore, $b_0\ll\omega_0$ and Eq. (36) is well approximated by the relation

$$\Delta\omega\approx\frac{b_0}{2}\,\mathrm{Im}\left[\frac{E_R}{E_S}\right] . \tag{37}$$

Thus, for a large range of normalized reflected field values, the frequency shift is on the order of the free-space radiative damping rate, indicating that $\Delta\omega\ll\omega_0$. This inequality has been assumed in the derivation of Eqs. (35) and (36). The possibility of large frequency shifts is addressed more carefully in Sec. IV when numerical results are considered.

III. THE ROTATIONALLY SYMMETRIC SOURCE POSITION

In this section, the capability of a spherical Bragg structure to enhance or inhibit source radiation is theoretically investigated for the simplest case. Specifically, the source is placed at the center of the structure ($r_0=0$). This case corresponds to a rotationally invariant geometry where the dipole moment orientation need not be specified. For dipole orientation $\hat{\vec{\alpha}}=\hat{\vec{z}}$ and position $r_0=0$, only the TM characteristic field component is necessary to determine the reflected electric field. A thorough examination of Eq. (31) shows that the TE characteristic fields vanish for this choice of dipole orientation due to the azimuthal symmetry of the dipole orientation.

From Eq. (32), the $\hat{\vec{\alpha}}=\hat{\vec{z}}$, the desired reflected field is given by the expression

$$E_R=\frac{1}{\varepsilon}\lim_{\vec{r}\to\vec{r}_0}[\hat{\vec{z}}\cdot\vec{D}_R^{\mathrm{TM}}(\vec{r})] . \tag{38}$$

The radial component of $\vec{D}_R^{\mathrm{TM}}$ is obtained by combining Eqs. (23) and (24)

$$\vec{r}\cdot\vec{D}_R^{\mathrm{TM}}(\vec{r})=O_S^{\mathrm{TM}}(\vec{r}_0)\sum_l\sum_m 2A_{lm}^{\mathrm{TM}}j_l(kr)Y_{lm}(\theta,\varphi) , \tag{39}$$

where the source differential operator $O_S^{\mathrm{TM}}(\vec{r}_0)$ is given by comparing Eqs. (19) and (21) and the constant reflected wave amplitude A_{lm}^{TM} is given by Eq. (28). For convenience, the explicit expressions for $O_S^{\mathrm{TM}}(\vec{r}_0)$ and A_{lm}^{TM} are provided below:

$$O_S^{\mathrm{TM}}(\vec{r}_0)=\frac{-kJ_0}{\omega_0}\hat{\vec{z}}\cdot\vec{\nabla}_0\times\vec{\nabla}_0\times\vec{r}_0 , \tag{40a}$$

$$A_{lm}^{\mathrm{TM}}=\frac{\rho_l^{\mathrm{TM}}j_l(kr_0)h_l^{(1)}(kr_1)Y_{lm}^*(\theta_0,\varphi_0)}{h_l^{(2)}(kr_1)-\rho_l^{\mathrm{TM}}h_l^{(1)}(kr_1)} . \tag{40b}$$

Substituting Eqs. (40a) and (40b) into Eq. (39) and performing the required differential operators, the radial component of $\vec{D}_R^{\mathrm{TM}}$ reduces to

$$\hat{\vec{r}}\cdot\vec{D}_R^{\mathrm{TM}}(\vec{r})=\sum_{l=0}^{\infty}12\pi\varepsilon E_S\frac{j_l(kr)}{kr}\left[\frac{\rho_l^{\mathrm{TM}}h_l^{(1)}(kr_1)}{h_l^{(2)}(kr_1)-\rho_l^{\mathrm{TM}}h_l^{(1)}(kr_1)}\right]\times\sum_{m=-l}^{l}\left[\cos\theta_0\left\{l(l+1)\frac{j_l(kr_0)}{kr_0}\right\}-\sin\theta_0\left\{\frac{j_l(kr_0)}{kr_0}+\frac{d}{d(kr_0)}j_l(kr_0)\right\}\frac{\partial}{\partial\theta_0}\right]Y_{lm}^*(\theta_0,\varphi_0)Y_{lm}(\theta,\varphi) . \tag{41}$$

As indicated by Eq. (38), it is necessary to evaluate Eq. (41) in the limit as $r\to r_0\to0$ due to the central position of the source. Furthermore, the angular limits require that $\theta\to\theta_0$ and $\varphi\to\varphi_0$. Logically, Eq. (38) must yield the same result regardless of the value of the source angular variables due to the degeneracy in these variables at the system origin. Thus it is expected that the angular dependence on the source variables apparent in Eq. (41) will not be present in the final field solution. To demonstrate this expected behavior, examine Eq. (41) in each of the three limits stated above. Beginning with the radial limit and excluding the $l=0$ case, it can be shown that

$$\lim_{r_0\to0}\frac{j_l(kr_0)}{kr_0}=\lim_{r_0\to0}\frac{d}{d(kr_0)}j_l(kr_0)=\tfrac{1}{3}\delta_{1l} , \tag{42}$$

where

$$\delta_{ll'}=\begin{cases}0, & l\neq l'\\ 1, & l=l' .\end{cases} \tag{43}$$

Applying Eq. (42) to Eq. (41), the following simplified equation results:

$$\hat{\vec{r}}\cdot\vec{D}_R^{\mathrm{TM}}(\vec{r})=\frac{8\pi\varepsilon E_S}{3}\left[\frac{\rho_1^{\mathrm{TM}}h_1^{(1)}(kr_1)}{h_1^{(2)}(kr_1)-\rho_1^{\mathrm{TM}}h_1^{(1)}(kr_1)}\right]\times\sum_{m=-1}^{1}\left[\cos\theta_0-\sin\theta_0\frac{\partial}{\partial\theta_0}\right]\times Y_{1m}^*(\theta_0,\varphi_0)Y_{1m}(\theta,\varphi) . \tag{44}$$

Performing the angular limits implied by Eq. (38) and noting that

$$\left[\cos\theta_0-\sin\theta_0\frac{\partial}{\partial\theta_0}\right]Y_{1m}^*(\theta_0,\varphi_0)=\left[\frac{3}{4\pi}\right]^{1/2}\delta_{0m} , \tag{45}$$

Eq. (44) yields

$$\hat{\vec{r}}\cdot\vec{D}_R^{\mathrm{TM}}(\vec{r}_0)=2\varepsilon E_S\left[\frac{\rho_1^{\mathrm{TM}}h_1^{(1)}(kr_1)}{h_1^{(2)}(kr_1)-\rho_1^{\mathrm{TM}}h_1^{(2)}(kr_1)}\right]\cos\theta_0\ , \tag{46}$$

where the explicit form for the spherical harmonic $Y_{10}(\theta_0,\varphi_0)$ was used.

The remaining task is to calculate the transverse field components from this characteristic component. This procedure is tedious, but straightforward through an application of Eqs. (29), (30), and (40) to yield

$$\hat{\vec{\theta}}\cdot\vec{D}_R^{\mathrm{TM}}(\vec{r}_0)=-2\varepsilon E_S\left[\frac{\rho_1^{\mathrm{TM}}h_1^{(1)}(kr_1)}{h_1^{(2)}(kr_1)-\rho_1^{\mathrm{TM}}h_1^{(1)}(kr_1)}\right]\sin\theta_0\ . \tag{47}$$

Thus the reflected field which does work on the source can be formed by projecting the dipole orientation vector onto the reflected field defined by Eqs. (46) and (47). Noting that $\hat{\vec{\alpha}}=\hat{\vec{z}}=\hat{\vec{r}}_0\cos\theta_0-\hat{\vec{\theta}}_0\sin\theta_0$, Eq. (38) yields the desired reflected electric field

$$E_R(r_0=0)=\left[\frac{2\rho_1^{\mathrm{TM}}h_1^{(1)}(kr_1)}{h_1^{(2)}(kr_1)-\rho_1^{\mathrm{TM}}h_1^{(1)}(kr_1)}\right]E_S\equiv\Gamma E_S\ , \tag{48}$$

where ρ_1^{TM} is determined by applying the vector coupled-wave theory of the companion paper and Γ is an effective reflection coefficient. The expressions for the normalized radiative damping rate and frequency shift can be formed by substituting Eq. (48) into Eqs. (35) and (37), respectively. Performing this substitution, the simple expressions below are obtained:

$$\frac{b}{b_0}=1+\mathrm{Re}(\Gamma)\ , \tag{49}$$

$$\Delta\omega\approx\frac{b_0}{2}\,\mathrm{Im}(\Gamma)\ . \tag{50}$$

Equations (49) and (50) are the expressions used in the next section to perform numerical calculations.

As expected, Eq. (48) is independent of both source and field angular variables. Furthermore, the form of this equation can be treated as a general result regardless of source position. Specifically, the reflected electric field at the source position is always factorable as an effective amplitude reflection coefficient multiplied by the source strength. For a given source position, Γ will generally consist of an infinite sum of TE and TM polarized waves and fully characterizes the effects of the Bragg cavity on the radiation from the source. For the centrally positioned source considered here, only a single term of the effective reflection coefficient series is nonzero due to the rotational invariance of the coupled system. The remaining computation is to determine the amplitude reflection coefficient of the $l=1$ harmonic for the TM polarization case ρ_1^{TM}. In general, however, this coefficient can only be calculated numerically as discussed in our companion paper. Finally, the $l=0$ case was excluded from the above analysis. For all source positions in the core region, it can be shown that this case does not contribute to the reflected field solution due to the dipole nature of the source radiation.

IV. NUMERICAL RESULTS AND DISCUSSION OF RADIATIVE EFFECTS DUE TO A SPHERICAL BRAGG STRUCTURE

Using the results of Sec. III, the capability of a spherical Bragg structure to enhance or inhibit dipole source radiation can be investigated numerically for some representative cases. The normalized radiative damping rate as a function of various parameters, such as the modulation, placement, and size of the Bragg structure, is of principal interest. The relative magnitudes of possible source frequency shifts are also examined to determine the validity of the assumption used in decoupling Eqs. (3) and (5).

For comparison to previous results, most notably the results from a line source in a cylindrical Bragg structure [13], a conventional notation for characterizing the source and structure is adopted. The vector spherical coupled-wave theory of our companion paper shows that the parameters that characterize a Bragg structure determine the reflectivity according to the coupling strength product κL, where

$$\kappa=kQ/4n_0^2\ . \tag{51}$$

To allow for maximum interaction with the Bragg structure, the source is exactly tuned to the Bragg frequency, or $\omega_0 n_0=\omega_B$, where

$$\omega_B=\pi c/\Lambda\ , \tag{52}$$

throughout much of the numerical analysis. The possibility for the cavity to appreciably shift the source frequency to significantly impact the calculated radiative lifetime of the source is one of several issues to be explored below.

Most of the cases considered below involve structures with only ten Bragg periods. This length is perhaps the lower limit that one might employ in any practical structure, since significant reflectivity from a ten-period structure requires large modulation or coupling constant κ. While this small number of periods is chosen for convenience to demonstrate possible cavity effects while minimizing computation time, the theory developed above is accurate for any modulation and Bragg region length. Even though coupled-wave theory is employed, the theory is not perturbative; synchronous or slowly varying envelope approximations are unnecessary. Also, most of the cases below place the beginning of the Bragg structure at least ten periods from the center, allowing for comparison with the calculations performed in Ref. [13].

The dependence of the normalized radiative damping rate on the inner radius of the Bragg region is first examined assuming that a centrally positioned source is exactly tuned to the Bragg frequency. As discussed in the companion paper, a phase term ϕ may be included in the argument of the sinusoid function which defines the square of the refractive index [Eq. (6)] such that

$$n^2(r)=\begin{cases}n_0^2+Q\sin[2\pi(r-r_1)/\Lambda-\phi]\ , & r_1<r<r_1+L\\ n_0^2 \quad \text{otherwise}\ .\end{cases} \tag{53}$$

However, it is not strictly accurate to vary the phase of the periodicity due to the introduction of index discontinuities, and thus additional reflections, at the end points of the Bragg region which are unaccounted for by the developed coupled-wave theory. It will be shown, however, that the results of the variation in the normalized radiative damping rate are nearly identical whether the phase or the inner radial position is varied. Furthermore, the error introduced by varying the phase and not accounting for the additional reflections is shown to be insignificant for the structures examined by a comparison to the results from a transfer-matrix method [17].

The normalized radiative damping rate, as defined in Eq. (49), is plotted as a function of the inner radius of the Bragg region in Fig. 1 for a source positioned at $r_0=0$. The Bragg region extends ten periods along the radial direction and three different coupling strengths are examined, denoted by $\kappa L=1$, 2, and 4. As the length of the Bragg region is constant for these curves, an increase in the κL product corresponds to an increase in the squared index modulation Q. Over most of the range of the inner radii examined, the source experiences inhibited radiation, since $b/b_0<1$. As the strength of the modulation increases, the size of this range and degree of inhibition similarly increase. There does exist, however, a range of r_1 that produces strongly enhanced emission. The magnitude of the enhancement resonance also increases with increasing Q, but becomes significantly sharper for stronger modulations.

As discussed above, varying the inner radius of the Bragg region, as in Fig. 1, is similar but not identical to varying the phase of the sinusoidal periodicity. In each case, the phase of the source wave with respect to the periodic structure is altered. However, in varying r_1/Λ, the refractive index remains continuous and additional reflections due to index discontinuities at r_1 and r_1+L need not be considered. An examination of Eq. (48) indicates that the qualitative results of Fig. 1 are nearly periodic with a period of $r_1/\Lambda=1$. Quantitatively, the phase and amplitude of Γ vary slowly between periods of r_1/Λ and approach asymptotic values for $kr_1\gg1$. The maximum (minimum) value of the normalized radiative damping rate in Fig. 1 will decrease (increase) between periods as the inner radius decreases and the resonant peak will shift to the left. The asymptotic behavior is expected as the source wave approaches its spherically symmetric limit and strongly interacts with the Bragg structure.

The normalized radiative damping rate is plotted as a function of the phase of the periodicity in Fig. 2(a). This rate functionally depends upon the $l=1$ TM amplitude reflection coefficient ρ_1^{TM} in Eq. (48). The two curves for

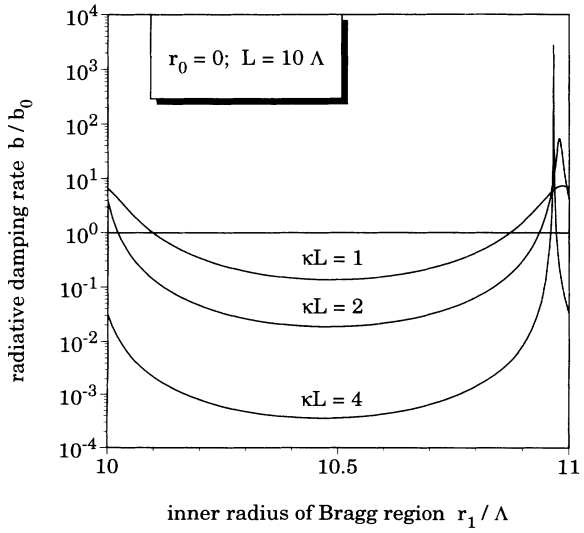

FIG. 1. Normalized radiative damping rate vs inner radius of Bragg region for a centrally positioned source.

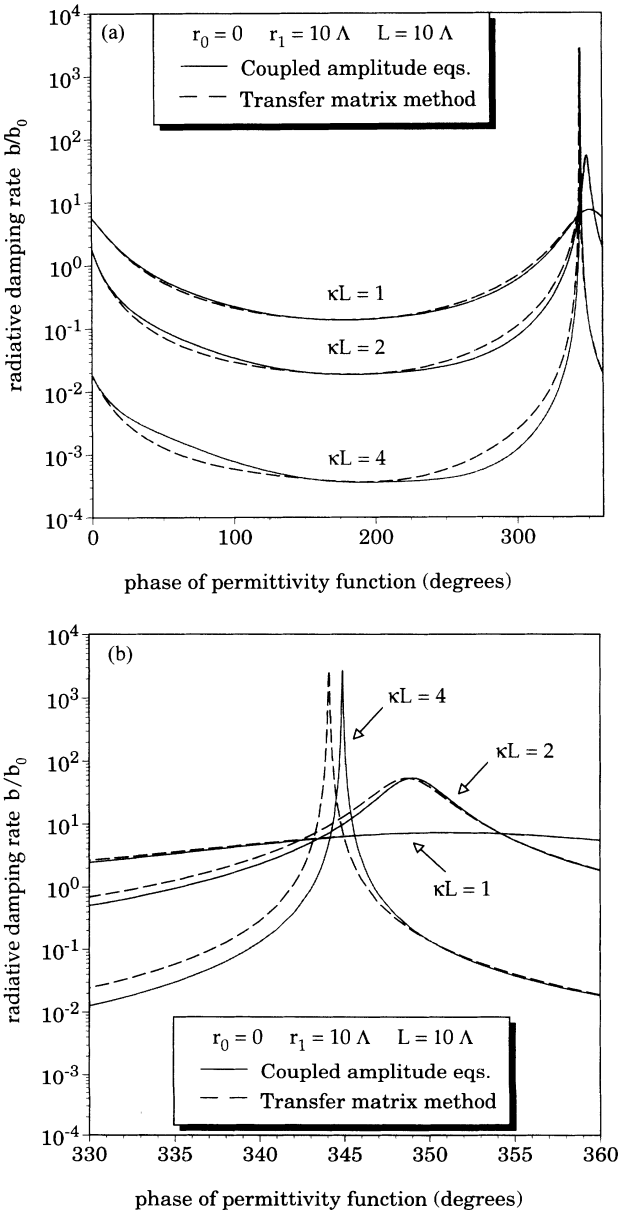

FIG. 2. (a) Normalized radiative damping rate vs phase of periodicity for a centrally positioned source. (b) Expanded view of (a).

each coupling product correspond to calculating this reflection coefficient by either coupled-mode theory or a transfer matrix method. The results from the two methods are nearly identical, with Fig. 2(b) illustrating on an expanded scale the slight, modulation-strength-dependent shift which occurs in the enhancement resonance. Note that the quantitative peak enhancement and inhibition values are essentially identical and that the curves of Fig. 2(a) behave in a manner nearly indistinguishable from the curves in Fig. 1. Thus, while most of the results presented in this paper involve variations in the position of the Bragg region, the results apply to a fixed-position Bragg structure with varying phase with only negligible error.

It is interesting to compare the results plotted in Figs. 1 and 2 to the results obtained in Ref. [13] for the dependence of the radiative damping rate on the phase for a line source centrally positioned in a cylindrical Bragg structure [19]. The features of the numerical analyses are nearly identical. In our companion paper, a dimensional scaling was noted from contradirectional coupling of circular waves in two dimensions to spherical waves in three dimensions. A consequence of this scaling is that the amplitude reflection coefficients used in the effective reflection coefficients are equal, to within a phase factor, in the asymptotic limit for the cylindrical and spherical Bragg structures. Conceptually, the cavity effects on the centrally positioned source for the two-dimensional and three-dimensional Bragg structures are similar. In the case of the cylindrical Bragg structure, a line source generates outward-traveling cylindrical waves which interact with a cylindrical structure. This is analogous to a point source which generates outward-traveling spherical waves which interact with a spherical structure. The comparison is not strictly valid due to the presence of a dipole source which does not radiate isotropically and to the vector nature of the interaction, but the two systems nevertheless remain very similar.

The next examination of the centrally positioned source geometry involves the variation in the normalized radiative damping rate as a function of coupling strength. Figure 3 shows b/b_0 plotted as a function of κL for several values of the inner radius of the periodic region. Fixing the squared index modulation, the length of the structure is varied. A few values of r_1 in the range $(r_1)_{\min} < r_1 < (r_1)_{\max}$ are selected, where $(r_1)_{\min}$ and $(r_1)_{\max}$ correspond to the minimum and maximum values, respectively, of b/b_0 for $\kappa L = 2$ in Fig. 1. The damping rate approaches zero (complete inhibition) as the length L of the periodic region increases. Note that a true maximum occurs for each inner radius value in Fig. 3, but that the asymptotic behavior ($b/b_0 \rightarrow 0$) with increasing κL is independent of r_1. This asymptotic behavior is similar to that of a photonic band-gap structure in which a band gap is created when the reflectivity of the Bragg structure approaches unity.

Figures 1 and 3 demonstrate that for $\kappa L = 4$, a spherical Bragg structure composed of only ten periods can inhibit the radiative decay rate by more than three orders of magnitude. The location r_1, as discussed above, and the magnitude of the squared index modulation Q play

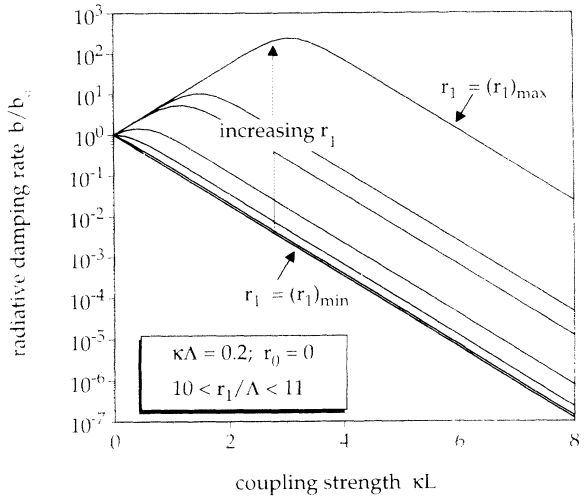

FIG. 3. Normalized radiative damping rate vs coupling strength for varying values of the inner radius. The source is centrally positioned and the permittivity modulation is fixed, thus varying the coupling strength is equivalent to varying the length of the Bragg region.

major roles. The larger the squared refractive index modulation, the smaller the value of L needed to achieve a specified level of inhibition. Consider the example of alternating layers of GaAs and AlAs, such as those used in a typical vertical-cavity semiconductor laser [20]. The squared refractive index difference corresponds to $Q \approx 3.76$, for which $\kappa\Lambda \approx 0.28$. For a central region one wavelength (2Λ) in diameter, an inhibition $b/b_0 \sim 1 \times 10^{-4}$ requires $\kappa L \sim 5$, so that $L/\Lambda \sim 18$ periods. This means a Bragg sphere of 38 periods in diameter, or approximately 6 μm at $\lambda_0 = 2n_0\Lambda = 0.98$ μm, can provide a nearly four-order-of-magnitude reduction in the dipole's radiative decay rate. An increase to an 8-μm-diam structure will produce an inhibition $b/b_0 \sim 1 \times 10^{-6}$. In general, a desired radiative damping rate and a maximum cavity diameter resulting from fabrication limitations can be specified. A set of universal curves with a specified Bragg interaction length L can then be generated to determine the necessary coupling constant κ and therefore the squared index modulation Q to achieve the desired degree of inhibition. Note that, in terms of Fig. 3, this set of universal curves would consist of various $(r_1)_{\min}$ curves of differing slopes which scale with the coupling constant. An example of these curves for the GaAs/AlAs material system is provided in Fig. 4.

The relatively small size associated with practically achievable squared refractive index differences is an encouraging sign. It will admittedly be challenging to fabricate photonic band-gap structures, but our calculations show that finite-size structures can indeed be expected to produce significant levels of inhibition. Some degree of caution is appropriate however. Not every materials system produces index changes (~ 0.58) as large as those of the GaAs/AlAs system considered here. For example, the core-cladding refractive index difference in a silica-based optical fiber is much smaller, typically of order 0.01. Much larger structures would be required in that case.

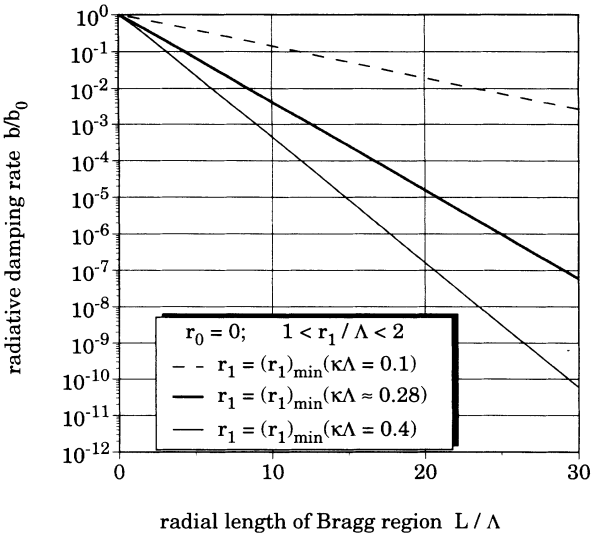

FIG. 4. Normalized radiative damping rate vs interaction length for varying values of the coupling constant. The source is centrally positioned and the inner radial position is chosen to give maximum inhibition (minimum enhancement) at the Bragg frequency.

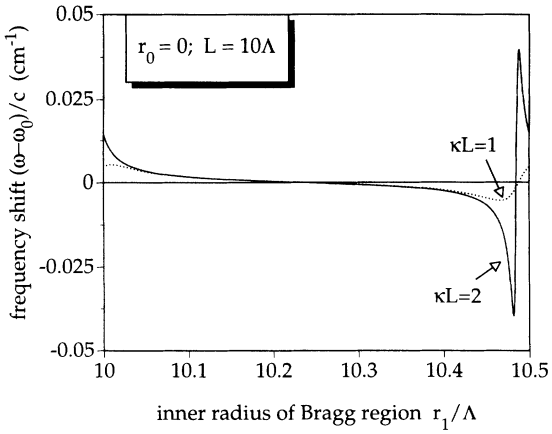

FIG. 6. Cavity-induced frequency shift of the dipole vs inner radius of Bragg region for a centrally positioned source.

For the above analysis, the assumption has been made that the source is always tuned to the Bragg frequency. A natural question to consider when using a Bragg cavity, however, is whether it is possible for the cavity to shift the frequency of the source enough to push it outside the reflection bandwidth of the cavity. If such a shift were possible, then the above numerical analysis would be invalidated by the interdependence of the normalized radiative damping rate and frequency shift. As shown below, it is an excellent approximation to assume that the cavity-induced frequency shift is negligible as far as Bragg-reflectivity effects are concerned.

In Fig. 5, the radiative damping rate as a function of frequency detuning from the Bragg frequency for a centrally located source is plotted. Assuming a Bragg structure designed for a source emitting at $\lambda_0/n_0 = 0.5\ \mu$m, so that $\Lambda = 0.25\ \mu$m, and fixed Bragg frequency, the source frequency $\omega = \omega_0 n_0$ is varied. The inner radial position is chosen to give maximum inhibition at the Bragg frequency. The plot shows expected oscillations in the damping rate, with the maximum inhibition occurring at the Bragg frequency. Note that the cavity resonances that produce local maxima in inhibition are more closely spaced for the weaker modulation case since the radial extent of the cavity is effectively larger due to the proportionality which exists between cavity reflectivity and Bragg region modulation. More importantly, the radiative damping rate does not change significantly over a range of frequencies greater than 1000 cm^{-1} ($\Delta\lambda > 4$ nm) around the Bragg frequency.

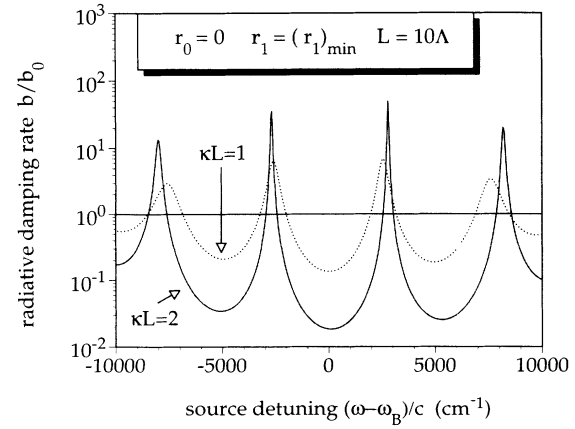

FIG. 5. Normalized radiative damping rate vs detuning of the source frequency from the Bragg frequency defined by the Bragg structure. The dipole source is placed at the center and the inner radial position is chosen to give maximum inhibition at the Bragg frequency.

Typical frequency shifts induced by the presence of the cavity are examined in Fig. 6. The plot of source frequency shift as a function of the inner radius of the Bragg region is qualitatively similar to Fig. 1 in terms of the characteristic resonance behavior. The source is again placed at the center to give an indication of the limiting range of possible frequency shifts for any source position. Even at resonance, the maximum frequency shift does not exceed ± 0.05 cm^{-1} for a modulation of $\kappa L = 2$. Comparing this value to the 1000 cm^{-1} range over which Bragg detuning can be considered negligible for calculations of the radiative damping rate, the assumption used above that the source always remains tuned to the Bragg frequency is reasonable.

V. CONCLUDING REMARKS

It has been shown that it is possible to either enhance or inhibit the emission of radiation from a dipole source located inside a spherically symmetric periodic structure for a centrally positioned source. Whether the source experiences enhancement or inhibition depends upon the position of the Bragg region with respect to the center of the spherical system. By altering this position, the phase of the source waves varies with respect to the phase of the periodic, index-modulated region. For the centrally

positioned source, the dipole tends to experience inhibition for most of the range of structure positions. A very narrow range of positions exists that leads to enhancements with the width of this range inversely proportional to the modulation strength. These quantitative results provide an understanding of the degree to which finite-size structures can inhibit or enhance the radiative decay rate. Furthermore, the generalized vector theory used to derive the above results can also be employed to examine the range of source positions about the central position in which appreciable radiative effects persist, an issue that lies outside the scope of this paper.

An analysis if the dipole source frequency shifts due to the presence of the spherical Bragg structure finds the shifts to be small. This analysis was performed only for a centrally positioned source, but this position, due to symmetry, represents the location of maximum coupling which can occur between the source and cavity. By comparing these shifts to the frequency range over which Bragg detuning can be considered negligible for calculations of the normalized radiative damping rate, it is found that the source remains nearly exactly tuned to the Bragg frequency even in cases of strong inhibition or enhancement of radiation. As with the results of the normalized radiative damping rate as a function of the inner radius of the Bragg region, the resultant frequency shifts for a centrally positioned source in a spherical Bragg structure are similar to those associated with a line source in a cylindrical Bragg structure. This similarity is another example of the scaling which occurs in dimensionality: from the coupling of cylindrical waves to a cylindrically symmetric cavity to the coupling of spherical waves to a spherically symmetric cavity.

In summary, we have determined the degree to which a finite-size, 3D Bragg structure can be expected to inhibit the radiation from a point dipole placed within it. Even though the calculation was carried out for a Bragg cavity possessing a great deal of symmetry, we believe the conclusions are broadly applicable. It is encouraging that only relatively small structures are needed to produce measurable changes in the radiative decay rate, provided the squared refractive index difference is sufficiently large. The classical theory we applied to this problem provides a connection between the relatively recent work on photonic band-gap structures and the earlier essentially one-dimensional work on the dipole-mirror problem, for which the same classical theory proved extremely successful.

ACKNOWLEDGMENTS

This research was supported in part by the National Science Foundation and the U.S. Army Research Office. K.G.S. wishes to thank O. King for many useful discussions and assistance in the generation of numerical results, and Dr. T. Erdogan for many helpful suggestions.

[1] E. M. Purcell, Phys. Rev. **69**, 681 (1946).
[2] S. Haroche and D. Kleppner, Phys. Today **42** (1), 24 (1989).
[3] D. Kleppner, Phys. Rev. Lett **47**, 233 (1981).
[4] R. G. Hulet, E. S. Hilfer, and D. Kleppner, Phys. Rev. Lett. **55**, 2137 (1985).
[5] K. H. Drexhage, in *Progress in Optics,* edited by E. Wolf (North-Holland, Amsterdam, 1974), Vol. 12, Chap. 4.
[6] W. R. Holland and D. G. Hall, Phys. Rev. Lett. **52**, 1041 (1984).
[7] D. G. Deppe and C. Lei, J. Appl. Phys **70**, 3443 (1991).
[8] Y. Yamamoto, S. Machida, and G. Björk, Phys. Rev. A **44**, 657 (1991); G. Björk, S. Machida, Y. Yamamoto, and K. Igeta, *ibid.* **44**, 669 (1991).
[9] H. Yokoyama, K. Nishi, T. Anan, H. Yamada, S. D. Brorson, and E. P. Ippen, Appl. Phys. Lett. **57**, 2814 (1990).
[10] E. Yablonovitch, Phys. Rev. Lett. **58**, 2059 (1987).
[11] P. R. Villeneuve and M. Piché, J. Opt. Soc. Am. A **8**, 1296 (1991).
[12] M. Plihal and A. A. Maradudin, Phys. Rev. B **44**, 8565 (1991).
[13] T. Erdogan, K. G. Sullivan, and D. G. Hall, J. Opt. Soc. Am. B **10**, 391 (1993).
[14] H. Kuhn, J. Chem. Phys. **53**, 101 (1970).
[15] R. R. Chance, A. Prock, and R. Silbey, in *Advances in Chemical Physics,* edited by I. Prigogine and S. A. Rice (Wiley, New York, 1978), Vol. 37, pp. 1–65.
[16] J. M. Wylie and J. E. Sipe, Phys. Rev. A **32**, 2030 (1985).
[17] W. C. Chew, *Waves and Fields in Inhomogeneous Media* (Van Nostrand Reinhold, New York, 1990), Chap. 3.
[18] W. K. H. Panofsky and M. Phillips, *Classical Electricity and Magnetism* (Addison-Wesley, Reading, MA, 1956), Chap. 20 and Eq. (21-3).
[19] The theoretical analysis of Ref. [13] contains an error due to the failure to incorporate the ratio of Hankel functions in the definition of the amplitude reflection coefficient. For the asymptotic regime of the numerical analysis, the result is a phase error which shifts the peak position of the normalized radiative damping rate as a function of the phase of the cylindrical Bragg structure.
[20] J. L. Jewell *et al.*, Appl. Phys. Lett. **55**, 424 (1989).